HHS Public Access

Author manuscript

Mol Imaging Biol. Author manuscript; available in PMC 2019 January 17.

Published in final edited form as:

Mol Imaging Biol. 2014 August ; 16(4): 586–594. doi:10.1007/s11307-014-0722-7.

Multimodal Imaging for Early Functional Response Assessment of ^{90}Y-/^{177}Lu-DOTATOC Peptide Receptor Targeted Radiotherapy with DW-MRI and ^{68}Ga-DOTATOC-PET/CT

Sarah Wulfert[1], **Clemens Kratochwil**[1], **Peter L. Choyke**[2], **Ali Afshar-Oromieh**[1], **Walter Mier**[1], **Hans-Ulrich Kauczor**[3], **Jens-Peter Schenk**[3], **Uwe Haberkorn**[1], and **Frederik L. Giesel**[1]

[1]Department of Nuclear Medicine, University Hospital Heidelberg, INF 400, 69120, Heidelberg, Germany

[2]Molecular Imaging Program, NCI, Bethesda, USA

[3]Department of Diagnostic and Interventional Radiology, University Hospital Heidelberg, Heidelberg, Germany

Abstract

Purpose: The purpose of this study is to investigate the utility of contrast-enhanced magnetic resonance imaging (CE-MRI), diffusion-weighted MRI (DW-MRI), and ^{68}Ga-DOTATOC positron emission tomography/computer tomography (^{68}Ga-DOTATOC PET/CT) in the assessment of response to loco-regional peptide receptor radiotherapy (PRRT) with ^{90}Y-/^{177}Lu-DOTATOC in patients with hepatic metastases from gastro-entero-pancreatic neuroen-docrine tumors (GEP-NET).

Procedures: CE-MRI, DW-MRI, and ^{68}Ga-DOTATOC-PET/CT images were acquired before and 3 months after one to two cycles of intra-arterial ^{90}Y-/^{177}Lu-DOTATOC therapy in 14 patients (nine female, five male; mean age, 54±9 years; range, 41–69 years) with hepatic metastases from GEP-NET. A total of 38 liver metastases were defined as target lesions for which the longest diameter, mean apparent diffusion coefficient (ADC_{mean}) and maximum standardized uptake value (SUV_{max}) were assessed. Based on changes in size on follow-up imaging, target lesions were classified as responding (RL) or nonresponding (NRL). Relative changes in tumor size, ADC_{mean}, and SUV_{max} were compared between the two subgroups.

Results: A total of 27 responding and 11 nonresponding lesions were successfully evaluated. Mean ADC_{mean} increased significantly in RL (p=0.011) as well as NRL (p=0.025). A significant correlation was found between baseline ADC_{mean} and both the percent ADC_{mean} change (p= 0.033) and decrease in lesion size after therapy (diameter p =0.006; volume p=0.002). SUV_{max} of RL declined significantly by 24.1 % (p =0.014) and remained nearly unchanged in NRL. The change of SUV_{max} correlated significantly with the pretreatment SUV_{max} (p<0.001) and the change in lesion diameter (p=0.009). NRL with an ADC_{mean} change >0.31×10^{-3} mm^2/s on first follow-up imaging showed a decrease in size in the long-term course.

Correspondence to: Frederik Giesel; frederik@egiesel.com.
Sarah Wulfert and Clemens Kratochwil contributed equally to this paper.

Conflict of Interest. There is no conflict of interest from the authors of this scientific work.

Conclusion: These results suggest that both DW-MRI and DOTATOC-PET imaging provide potential biomarkers for early assessment of treatment and stratification of therapy response, but that DW-MRI should be interpreted only in combination with SSTR expression and morphologic changes.

Keywords

Peptide receptor-targeted radiotherapy; Multimodal imaging; Neuroendocrine cancer; Response monitoring; 68Ga-DOTATOC PET; DW-MRI

Introduction

Although rare, neuroendocrine tumors (NET) have steadily increased in frequency over the last 30 years, mainly due to raised awareness and improved diagnostics [1–6]. Gastro-entero-pancreatic neuroendocrine tumors (GEP-NET) represent approximately 75 % of all NET [7]. This entity often presents with liver metastases, which is a strongly negative prognostic indicator [8, 9]. Thus, in the recent years many efforts have been made to optimize the therapy of inoperable focal GEP-NET liver metastases [10–12]. Besides the advancements in conventional therapeutic procedures such as percutaneous ablative therapies, surgical resection or trans-arterial chemotherapy, there has been notable progress in customized palliative therapies for metastatic GEP-NET utilizing targeted therapeutic radio-pharmaceuticals [13–16].

A relatively new approach in this domain is to utilize peptide receptor radionuclide therapy (PRRT) by chelating ^{90}Y or ^{177}Lu to DOTA(0)-Phe(1)-Tyr(3)-octreotide (DOTA-TOC) and injecting it selectively into the hepatic artery [17, 18]. Most GEP-NET primaries and metastases demonstrate increased expression of somatostatin receptor [19, 20]. Thus, the radiolabeled somatostatin analog DOTATOC targets malignant tissue with relatively minor damage to surrounding healthy structures. However, the assessment of response to this treatment remains a challenging task, as it primarily induces tumor lysis and a loss of cellular integrity which may not immediately result in reduced tumor size [21]. Thus, additional methods are needed to determine early responses to this locoregional therapy. In this study, we analyzed diffusion-weighted magnetic resonance imaging (DW-MRI) and ^{68}Ga-DOTATOC positron emission tomography/computer tomography (^{68}Ga-DOTATOC PET/CT) images to determine if functional imaging could provide an early indicator of tumor response to PRRT.

Patients and Methods

Thirty-six patients with refractory hepatic metastases from GEP-NET were treated with intra-arterial ^{90}Y-/^{177}-Lu-DOTATOC. Institutional review board approval was obtained. All patients provided informed consent. Fourteen of these patients (nine female, five male; mean age, 54±9 years; range, 41–69 years) underwent DW-MRI before and after one to two cycles of intra-arterial PRRT and were thus included in this retrospective study. For 11 of these 14 patients, PET/CT images at the same time points were also available for review. Of the 14 patients, eight had a neuroendocrine tumor of the pancreas, four of the intestine, one of the stomach, and one patient had a neuroendocrine tumor of unknown primary. Eight of the 14

patients had already undergone one to three cycles of conventional intravenous PRRT without sufficient response. In order to minimize bias, no more than three hepatic lesions (>2 cm longest diameter) per patient were analyzed. The measurement of mean apparent diffusion coefficient (ADC_{mean}) values had to be possible on at least three consecutive sections for each metastasis on the baseline DW-MRI. During the follow-up period, none of the patients received concomitant treatments except symptomatic therapy with somatostatin analogs.

Catheter Placement and Treatment Regimen

A 4-French catheter (Sidewinder S1) was placed in the celiac artery *via* transfemoral access using the Seldinger technique with local anesthesia. Subsequently, a microcatheter (Progreat) was inserted coaxially and advanced to the common hepatic artery or proper hepatic artery. In cases of anatomic variation, the largest arterial feeder was cannulated. The catheter was used to deliver ^{90}Y- and/or ^{177}Lu-DOTATOC. To minimize renal toxicity, 1,000 ml of a nephroprotective solution containing 30 g lysine and 30 g arginine was applied simultaneously.

MR Imaging Technique and Analysis

Magnetic resonance examinations were performed on a 1.5-T MR system (Avanto, Siemens Medical Systems, Erlangen, Germany). Unenhanced T1-weighted (gradient echo, TR=192 ms, TE= 4.76 ms, 256×154 matrix) and T2-weighted (HASTE, TR= 801 ms, TE=69 ms, 384×213 matrix) fast spin echo axial imaging was performed before DW-MRI and Gd-EOB-DTPA (Primovist®, Bayer Schering, Berlin, Germany) administration for contrast-enhanced magnetic resonance imaging (CE-MRI). DW-MRI was performed with a breath-hold single-shot echo planar sequence (TR=12,200 ms; TE=67 ms; FOV 430 cm; section thickness5 mm; *b* values 50, 300, and 600 s/mm^2; voxel 3.3×3.3×5, EPI factor 112).

The acquisition of delayed postcontrast MR data started with the i.v. administration of 0.1 mmol/kg body weight of the contrast agent Gd-EOB-DTPA with an infusion rate of 1.5 ml/s followed by a 30-ml saline bolus. Imaging was performed with a T1w volumetric interpolated breath hold examination (VIBE) with 3.41 ms TR, 1.18 ms TE, 4 mm slice thickness, 320× 180 matrix, and 72 axial slices with an acquisition time of 20 s for each dataset.

Two to three target lesions per patient were selected in the hepatocyte specific contrast phase 15 min p.i. (late enhanced) which was considered the gold standard for lesion delineation on the baseline examination and then were followed on the later MRI [5]. Because of the favorable tumor to liver contrast, the longest diameter (LD) of each lesion was manually measured on late-enhanced MR images. For the assessment of tumor volume, the workstation Ziostation® (Ziosoft Inc., Redwood City, USA) was used. After manual delineation of the lesions' borders on several slices, an automatic interpolation and calculation of tumor volume in cubic centimeters was acquired by the software.

DW-MRI data was analyzed using in-house developed software (DKFZ, Heidelberg, Germany) based on Interactive Data Language (IDL, Exelis Visual Information Solutions, Boulder, CO, USA). For each target metastasis, regions of interest (ROI) were placed in

three different layers, covering as much of the lesion as possible. For each layer, the ADC_{mean} was calculated by the software using the formula $S=S_0 \exp(-b \cdot ADC)$. Using the three b values (b=50, 300, and 600 s/mm^2), a nonlinear Levenberg–Marquardt fit was used to calculate S_0 and ADC_{mean}. The mean value of the three measurements per lesion was taken as the representative value for further analysis. Additionally, ADC_{mean} values of normal-appearing liver parenchyma and spleen were assessed in the same manner for every patient. ADC is a marker for the diffusion of water molecules based on Brownian motion. As it is inversely proportional to the cellularity of biological tissue, ADC values are high in necrotic areas with unrestricted diffusion and are low in vital tissues with high cell density and intact cell membranes such as viable tumor. After anticancer therapies, fibrotic remodeling can also lead to a decrease in ADC, whereas apoptosis and therapy-induced necrosis increase the ADC.

PET/CT Imaging Technique and Image Analysis

The PET studies were acquired with a Biograph 6 PET/CT (Siemens Medical Systems, Erlangen, Germany). Imaging was started 40±10 min after the i.v. injection of 84–196 MBq of ^{68}Ga-DOTATOC. Static emission scans—corrected for dead time, scatter, and decay—were acquired from the vertex to the proximal legs, requiring eight bed positions (4 min each). Contrast-enhanced CT (CE-CT) was performed as a part of the PET/CT. The iodinated contrast medium (Imeron 400, Bracco Diagnostics, Milan, Italy) was injected at a flow rate of 4 ml/s. The liver and abdomen were initially examined without contrast media (130 keV, 30 mAs, CareDose), followed by an arterial phase (25 s delay) and a portal venous phase (60 s delay). The low-dose CT without contrast agent was used for attenuation correction. Slice collimation was 6×1.0 mm, pitch factor 1.5, 110 keV, 95 mAs (CareDose), matrix 512×512, rotation time 0.6 s, reconstructed to a slice thickness of 1.25- and 0.8-mm increment with a B30-kernel. Secondary raw data were reformatted to a slice thickness of 5 mm with a 2.5 mm increment in the coronal and axial view. The images were iteratively reconstructed with the ordered subset expectation maximization (OSEM) algorithm using four iterations with eight subsets and Gaussian filtering to achieve an in-plane spatial resolution of 5 mm at full-width half-maximum. Calculation of the maximum standardized uptake value (SUV_{max}) of a target lesion was performed after identification of the lesion on both PET/CT and MRI. Circular ROIs were drawn around these areas of increased uptake in transaxial slices and automatically adapted by e.soft software (Siemens Medical Systems, Erlangen, Germany) to a three-dimensional volume, in which the SUV_{max} was determined automatically by the software. Analogously, the SUV_{max} of normal-appearing liver parenchyma and spleen was evaluated after placing a ROI into a region without tumor infiltration (the region for normal liver parenchyma was selected after double checking with MRI, CT, and PET).

Assessment of Therapeutic Response

For each metastatic lesion, the following data was assessed: tumor volume (TV), LD, ADC_{mean}, and SUV_{max} before and after treatment. Response to therapy was determined on a lesion-by-lesion basis by evaluating changes in metastasis size between baseline and follow-up MRI. A metastasis was classified as responding lesion (RL) if its LD decreased or did not change and nonresponding lesion (NRL) if the tumor diameter increased.

Statistical Analysis

All statistical analysis was carried out with the free software environment “R”. A p value of 0.05 was considered statistically significant. The quantified variables are described as median and interquartile range (IQR) or as percentages for discrete variables. For data comparison within the same groups, the Wilcoxon signed-rank test for related samples was applied. Intergroup comparisons were performed with the Mann–Whitney test for independent samples. Correlations between the assessed parameters (LD, TV, SUV, and ADC_{mean}) and between their percent changes from baseline were determined using Spearman’s rank correlation coefficient.

Results

Thirty-eight metastases were defined based on delayed enhanced MRI as target lesions. Thirty-seven of these target lesions could be identified and analyzed on baseline DW-MR images. Of the 11 patients with PET/CT data available, all 29 of their target lesions as identified on CE-MRI were present on the baseline PET/CT. Due to therapy response, two of 37 target lesions could not be identified on DW-MRI after PRRT. According to changes in lesion size, 27 metastases (71 %) were classified as RL and 11 metastases (29 %) as NRL. Before therapy, LD of RL was 30.4 mm (IQR, 13.4) and the LD of NRL 33.2 mm (IQR, 18.2). There was no significant difference between the median pretreatment size of the two groups (p=0.159). Baseline TV of RL was 9.6 cm^3 (IQR, 7.9) and for NRL was 18.1 cm^3 (IQR, 39.9; p=0.147). On follow-up MRI 3 months after the last treatment cycle, the LD of RL decreased significantly by 11.2 % (IQR, 21.5; p<0.001), whereas NRL showed a LD increased significantly by 8.5 % (IQR, 16.4; p<0.001).

The initial ADC_{mean} of RL was 1.21×10^{-3} mm^2/s (IQR, 0.61) and of NRL 1.09×10^{-3} mm^2/s (IQR, 0.35; p=0.392). On follow-up DW-MRI, ADC_{mean} increased significantly both in RL (+10.6 %; IQR, 38.8; p=0.011) and in NRL (+18.1 %; IQR, 27.3; p=0.025) with the percentage of change in ADC_{mean} values of NRL being higher than those of RL (Figs. 1a and 2). Baseline ADC_{mean} of all lesions correlated weakly but significantly negative both with LD (r=−0.441; p=0.006) and TV (r=−0.500; p=0.002).

Although most RL demonstrated an increase in ADC_{mean} after PRRT, seven lesions were found to decrease in ADC_{mean} value by a mean of −26.8 % (Fig. 2).

Additionally, the ADC_{mean} of normal liver parenchyma (n =14) and of the spleen (n = 11) was assessed. Three patients had undergone prior splenectomy. Neither the ADC_{mean} values of normal liver parenchyma nor of spleen tissue showed a significant change after therapy (p>0.05).

On PET/CT images, 29 of the target metastases could be analyzed before and 27 after therapy. Baseline median SUV_{max} of RL was 28.48 and decreased by 24.1 % on follow-up PET/CT (p=0.014), whereas SUV_{max} of NRL (baseline, 22.03) increased by 3.9 % (p=0.910; n.s.; Fig. 1b). Baseline SUV_{max} of the two subgroups did not show a significant difference. A negative correlation was observed between pretreatment SUV_{max} and the

percent change of SUV_{max} after therapy (r=−0.769; p<0.001) as well as with the percent change of LD (r=−0.482; p=0.009) and TV (r=−0.516; p=0.005).

The SUV_{max} of spleen tissue increased significantly by a median of 24.3 % (p=0.039) during the observation period, whereas the SUV_{max} of normal liver parenchyma showed no significant changes. The change of SUV_{max} in the spleens did not correlate significantly with change of SUV_{max} in the target lesions.

Table 1 provides a short overview over the results listed above. Figures 3 and 4 show an example of a responding lesion and of a nonresponding lesion, respectively, before and after PRRT.

As our results showed a stronger increase of ADC_{mean} in NRL than in RL after the first follow-up, we analyzed the 11 NRL again later in the course of treatment. All of the 11 NRL could be analyzed on a second follow-up imaging with CEMRI in mean 6 months after first follow-up. The examined patients had undergone further intra-arterial DOTATOC therapy in the interval. Three of the NRL finally decreased in size, while eight had grown compared to the baseline LD.

In the three lesions that demonstrated a decrease in size and volume, a mean ADC_{mean} increase of 29.0 % from baseline to first follow-up and a mean decrease in SUV_{max} of 19.0 % was observed (Fig. 5). The eight growing lesions demonstrated an increase in ADC_{mean} of 12.0 % from baseline to first follow-up. In five of these eight lesions, PET/CT data was available (baseline and follow-up). Here, a mean increase of SUV_{max} of 22.4 % was measured. Due to the small number of cases, we refrained from a statistical analysis of this finding.

Discussion

In this retrospective study, the ADC_{mean} of neuroendocrine liver metastases increased significantly both in RL and in NRL. Before therapy, there was no significant difference in the ADC_{mean} of the two groups. Baseline-ADC_{mean} of the assessed target lesions correlated inversely with the percent change of LD (r=−0.44; p=0.006) and volume (r=−0.50; p=0.002) under PRRT. This shows that the higher the ADC_{mean} before therapy, the more the metastases decreased in size. In other studies, patients with a higher baseline ADC showed a worse response to therapy. Koh *et al.* [22] investigated hepatic metastases of colorectal cancer under chemotherapy and noted a significantly higher ADC in nonresponding lesions before therapy than in responding lesions (p=0.002). They also found an inverse correlation of baseline ADC and percent reduction in lesion size (r=−0.58; p=0.03). Cui *et al.* [23] also showed an inverse correlation of these values for the same tumor entity but under concomitant chemoradiotherapy (r=−0.293; p=0.006). It is assumed that tumors with higher baseline ADC have some necrotic areas, which could indicate hypoxia mediated radioresistance. However, this hypothesis cannot be generalized for all tumor entities. In a study by DeVries *et al.* [24], no differences between baseline ADC value was found for responders and nonresponders in rectal carcinoma, as is also the case in our study.

Seven responding lesions had decreased ADC_{mean} values after PRRT. Further assessment of these target lesions demonstrated that they had a high mean pretherapy ADC_{mean} of 1.81×10^{-3} mm^2/s with four of the lesions having a baseline ADC_{mean} of $>2.0\times10^{-3}$ mm^2/s. It is possible that the ADC_{mean} change is related to fibrosis as these lesions also exhibited marked reductions in size.

In general, a low ADC is associated with high cell density [25, 26] and low water diffusivity (Fig. 6). This could negatively affect the saturation of somatostatin-receptors (SSTR) with ^{90}Y-/^{177}Lu-DOTATOC because the ability of the radiopeptide to diffuse in densely packed cells could be hindered. As the uptake of radiolabeled DOTATOC is essential for inducing radiation damage in tumor tissue [17, 27, 28], this could explain why there was a minor response in lesions with high cell density. This thesis is supported by the significant correlation of ADC_{mean} and SUV_{max} before therapy (r=0.50; p=0.007). At higher baseline ADC_{mean}—and thus lower cell density—we found a higher uptake of ^{68}Ga-DOTATOC in PET/CT. In future studies, the additional evaluation of minimum ADC (ADC_{min}) could be of interest, as this value has shown a correlation to SUV_{max} in a very recent study [29]. Further investigation will be needed to determine the impact of ADC_{min} assessment.

In our study, the ADC_{mean} of RL and NRL increased significantly under PRRT. This increase can either be ascribed to therapy-induced cell damage or to new intrametastatic necrotic areas which spontaneously arise in proliferating tumors. The differentiation between these two options is challenging [30, 31]. In RL, the increase in ADC_{mean} was accompanied by a decrease in SUV_{max}, which implies a cell loss due to PRRT. In NRL, the rise of ADC_{mean} came along with tumor growth and an increase in SUV_{max}. Conceivably, there can be a combination of newly formed necrotic areas that increase the ADC_{mean} and proliferating vital tumor tissue which causes the lesions' growth and the higher uptake of ^{68}Ga-DOTATOC.

The ADC_{mean} of normal liver tissue and spleen showed no significant differences after therapy. This speaks for the specific impact of the PRRT on tumor tissue while sparing healthy surrounding structures.

Before therapy, the SUV_{max} of RL was higher than the SUV_{max} of NRL; however, the difference was not significant. Gabriel *et al.* [32] also found no significant difference in baseline SUV_{max} of responders and nonresponders in their study evaluating the efficacy of intravenous PRRT with ^{68}Ga-DOTATOC-PET. Campana *et al.* [33] investigated the role of ^{68}Ga-DOTANOC uptake as a prognostic factor in neuroendocrine tumors. Patients with partial remission or stable disease showed a significantly higher SUV_{max} than patients with progressive disease.

In our study, the baseline SUV_{max} of the target lesions correlated inversely with the percent change of LD, volume, and SUV_{max} under PRRT. A higher pretreatment SUV_{max} was associated with a greater decrease of lesion size and SUV_{max} during therapy. These results are endorsed by the report of Koukouraki *et al.* [34], in which an elevated baseline SUV_{max} was associated with higher binding of ^{68}Ga-DOTATOC on SSTR2 and thus with a favorable effect of PRRT.

SUV_{max} of RL decreased by 24.1 % whereas it increased by 3.9 % in NRL. A significant correlation was found between percent change of LD/volume and percent change of SUV_{max} under PRRT. Therefore, a decrease in lesion size often was accompanied by a decrease of SUV_{max} and *vice versa*. Kroiss *et al.* [35] also found a lower SUV_{max} in hepatic metastases under PRRT, and Gabriel *et al.* [32] reported a higher relative decrease of ^{68}Ga uptake under systemic PRRT in responders than in nonresponders.

However, Gabriel *et al.* [32] could not find clear correlations of SUV values with outcome parameters. In this study, the decrease in SUV_{max} under PRRT with concomitant shrinking of the target lesions can probably be ascribed to necrosis and apoptosis of tumor cells. The second follow-up of the nonresponding lesions showed that lesions with a decrease in SUV_{max} after the first follow-up also eventually decreased in size after longer time periods. The percentage decrease of SUV_{max} under PRRT could thus suggest therapy response.

In this study, the SUV_{max} of the spleen (n=8) rose by 34.0 % in the observation period, whereas the ^{68}Ga-DOTATOC uptake in the liver remained stable. Haug *et al.* [36] reported already that PRRT can influence the ^{68}Ga-DOTATATE uptake in neuroendocrine tumors and the spleen with the SUV_{max} in the spleen being lower before therapy. The leading thought here is that a successful PRRT reduces the tracer uptake specifically in the tumor and hence more tracer is left in the blood stream for physiological uptake in the spleen and other organs. This is supported by the observation of an unchanged ADC_{mean} in the spleen.

Conclusion

High initial SUV_{max} values in ^{68}Ga-DOTATOC-PET as well as high ADC_{mean} values in DW-MRI both suggest better therapeutic response to PRRT. A decrease in SUV_{max} in DOTATOC-PET is a good surrogate for early response assessment after one to two cycles of therapy. In contrast, DW-MRI presents both treatment-induced tumor necrosis and a higher tumor cellularity due to continuing tumor growth resulting in the same changes of ADC_{mean} values. Therefore, in the setting of NET, the ADC_{mean} value—while a promising biomarker—should be interpreted only in combination with SSTR expression or imaging morphology.

Acknowledgements.

We highly appreciate the support of PD Dr. S. Ley in DWI sequence adaptation and Dr. T. Kuder in DWI sequence analysis.

References

1. Schimmack S, Svejda B, Lawrence B et al. (2011) The diversity and commonalities of gastroenteropancreatic neuroendocrine tumors. Lan-genbecks Arch Surg 396:273–298
2. Lawrence B, Gustafsson BI, Chan A et al. (2011) The epidemiology of gastroenteropancreatic neuroendocrine tumors. Endocrinol Metab Clin North Am 40:1–18, vii [PubMed: 21349409]
3. Oberg K, Castellano D (2011) Current knowledge on diagnosis and staging of neuroendocrine tumors. Cancer Metastasis Rev 30(Suppl 1):3–7 [PubMed: 21311954]
4. Yao JC, Hassan M, Phan A et al. (2008) One hundred years after “carcinoid”: epidemiology of and prognostic factors for neuroendocrine tumors in 35,825 cases in the United States. J Clin Oncol 26:3063–3072 [PubMed: 18565894]

5. Giesel FL, Kratochwil C, Mehndiratta A et al. (2012) Comparison of neuroendocrine tumor detection and characterization using DOTATOC-PET in correlation with contrast enhanced CT and delayed contrast enhanced MRI. Eur J Radiol 81:2820–2825 [PubMed: 22236704]
6. Giesel FL, Wulfert S, Zechmann CM et al. (2013) Contrast-enhanced ultrasound monitoring of perfusion changes in hepatic neuroendocrine metastases after systemic *versus* selective arterial 177Lu/90Y-DOTATOC and 213Bi-DOTATOC radiopeptide therapy. Exp Oncol 35:122–126 [PubMed: 23828389]
7. Pape UF, Bohmig M, Berndt U et al. (2004) Survival and clinical outcome of patients with neuroendocrine tumors of the gastroenter-opancreatic tract in a german referral center. Ann N Y Acad Sci 1014:222–233 [PubMed: 15153439]
8. Modlin IM, Lye KD, Kidd M (2003) A 5-decade analysis of 13,715 carcinoid tumors. Cancer 97:934–959 [PubMed: 12569593]
9. Ghevariya V, Malieckal A, Ghevariya N et al. (2009) Carcinoid tumors of the gastrointestinal tract. South Med J 102:1032–1040 [PubMed: 19738517]
10. Roche A, Girish BV, de Baere T et al. (2003) Trans-catheter arterial chemoembolization as first-line treatment for hepatic metastases from endocrine tumors. Eur Radiol 13:136–140 [PubMed: 12541121]
11. Pitt SC, Knuth J, Keily JM et al. (2008) Hepatic neuroendocrine metastases: chemo- or bland embolization? J Gastrointest Surg 12:1951–1960 [PubMed: 18709512]
12. Vogl TJ, Naguib NN, Zangos S et al. (2009) Liver metastases of neuroendocrine carcinomas: interventional treatment *via* transarterial embolization, chemoembolization and thermal ablation. Eur J Radiol 72:517–528 [PubMed: 18829195]
13. Nazario J, Gupta S (2010) Transarterial liver-directed therapies of neuroendocrine hepatic metastases. Semin Oncol 37:118–126 [PubMed: 20494704]
14. Mayo SC, de Jong MC, Pulitano C et al. (2010) Surgical management of hepatic neuroendocrine tumor metastasis: results from an international multi-institutional analysis. Ann Surg Oncol 17:3129–3136 [PubMed: 20585879]
15. Strosberg JR, Cheema A, Kvols LK (2011) A review of systemic and liver-directed therapies for metastatic neuroendocrine tumors of the gastroenteropancreatic tract. Cancer Control 18:127–137 [PubMed: 21451455]
16. McStay MK, Maudgil D, Williams M et al. (2005) Large-volume liver metastases from neuroendocrine tumors: hepatic intraarterial 90Y-DOTA-lanreotide as effective palliative therapy. Radiology 237:718–726 [PubMed: 16192318]
17. Kratochwil C, Giesel FL, Lopez-Benitez R et al. (2010) Intraindividual comparison of selective arterial *versus* venous 68Ga-DOTATOC PET/CT in patients with gastroenteropancreatic neuroendocrine tumors. Clin Cancer Res 16:2899–2905 [PubMed: 20460485]
18. Kratochwil C, Lopez-Benitez R, Mier W et al. (2011) Hepatic arterial infusion enhances DOTATOC radiopeptide therapy in patients with neuroendocrine liver metastases. Endocr Relat Cancer 18:595–602 [PubMed: 21791571]
19. Reubi JC, Waser B (2003) Concomitant expression of several peptide receptors in neuroendocrine tumours: molecular basis for *in vivo* multi-receptor tumour targeting. Eur J Nucl Med Mol Imaging 30:781–793 [PubMed: 12707737]
20. de Herder WW, Hofland LJ, van der Lely AJ et al. (2003) Somatostatin receptors in gastroentero-pancreatic neuroendocrine tumours. Endocr Relat Cancer 10:451–458 [PubMed: 14713257]
21. Forner A, Ayuso C, Varela M et al. (2009) Evaluation of tumor response after locoregional therapies in hepatocellular carcinoma: are response evaluation criteria in solid tumors reliable? Cancer 115:616–623 [PubMed: 19117042]
22. Koh DM, Scurr E, Collins D et al. (2007) Predicting response of colorectal hepatic metastasis: value of pretreatment apparent diffusion coefficients. AJR Am J Roentgenol 188:1001–1008 [PubMed: 17377036]
23. Cui Y, Zhang XP, Sun YS et al. (2008) Apparent diffusion coefficient: potential imaging biomarker for prediction and early detection of response to chemotherapy in hepatic metastases. Radiology 248:894–900 [PubMed: 18710982]

24. DeVries AF, Kremser C, Hein PA et al. (2003) Tumor microcirculation and diffusion predict therapy outcome for primary rectal carcinoma. Int J Radiat Oncol Biol Phys 56:958–965 [PubMed: 12829130]
25. Herneth AM, Guccione S, Bednarski M (2003) Apparent diffusion coefficient: a quantitative parameter for *in vivo* tumor characterization. Eur J Radiol 45:208–213 [PubMed: 12595105]
26. Patterson DM, Padhani AR, Collins DJ (2008) Technology insight: water diffusion MRI—a potential new biomarker of response to cancer therapy. Nat Clin Pract Oncol 5:220–233 [PubMed: 18301415]
27. Kaltsas GA, Papadogias D, Makras P et al. (2005) Treatment of advanced neuroendocrine tumours with radiolabelled somatostatin analogues. Endocr Relat Cancer 12:683–699 [PubMed: 16322317]
28. Reubi JC (2004) Somatostatin and other peptide receptors as tools for tumor diagnosis and treatment. Neuroendocrinology 80(Suppl 1):51–56 [PubMed: 15477718]
29. Rakheja R, Chandarana H, Demello L et al. (2013) Correlation between standardized uptake value and apparent diffusion coefficient of neoplastic lesions evaluated with whole-body simultaneous hybrid PET/MRI. AJR Am J Roentgenol 201:1115–1119 [PubMed: 24147485]
30. Cha J, Kim ST, Kim HJ et al. (2013) Analysis of the layering pattern of the apparent diffusion coefficient (ADC) for differentiation of radiation necrosis from tumour progression. Eur Radiol 23:879–886 [PubMed: 22903642]
31. Thoeny HC, Ross BD (2010) Predicting and monitoring cancer treatment response with diffusion-weighted MRI. J Magn Reson Imaging 32:2–16 [PubMed: 20575076]
32. Gabriel M, Decristoforo C, Kendler D et al. (2007) 68Ga-DOTA-Tyr3-octreotide PET in neuroendocrine tumors: comparison with somatostatin receptor scintigraphy and CT. J Nucl Med 48:508–518 [PubMed: 17401086]
33. Campana D, Ambrosini V, Pezzilli R et al. (2010) Standardized uptake values of (68)Ga-DOTANOC PET: a promising prognostic tool in neuroendocrine tumors. J Nucl Med 51:353–359 [PubMed: 20150249]
34. Koukouraki S, Strauss LG, Georgoulias V et al. (2006) Evaluation of the pharmacokinetics of 68Ga-DOTATOC in patients with metastatic neuroendocrine tumours scheduled for 90Y-DOTATOC therapy. Eur J Nucl Med Mol Imaging 33:460–466 [PubMed: 16437218]
35. Kroiss A, Putzer D, Decristoforo C et al. (2013) (68)Ga-DOTA-TOC uptake in neuroendocrine tumour and healthy tissue: differentiation of physiological uptake and pathological processes in PET/CT. Eur J Nucl Med Mol Imaging 40(4):514–523 [PubMed: 23291643]
36. Haug AR, Auernhammer CJ, Wangler B et al. (2010) 68Ga-DOTA-TATE PET/CT for the early prediction of response to somatostatin receptor-mediated radionuclide therapy in patients with well-differentiated neuroendocrine tumors. J Nucl Med 51:1349–1356 [PubMed: 20720050]

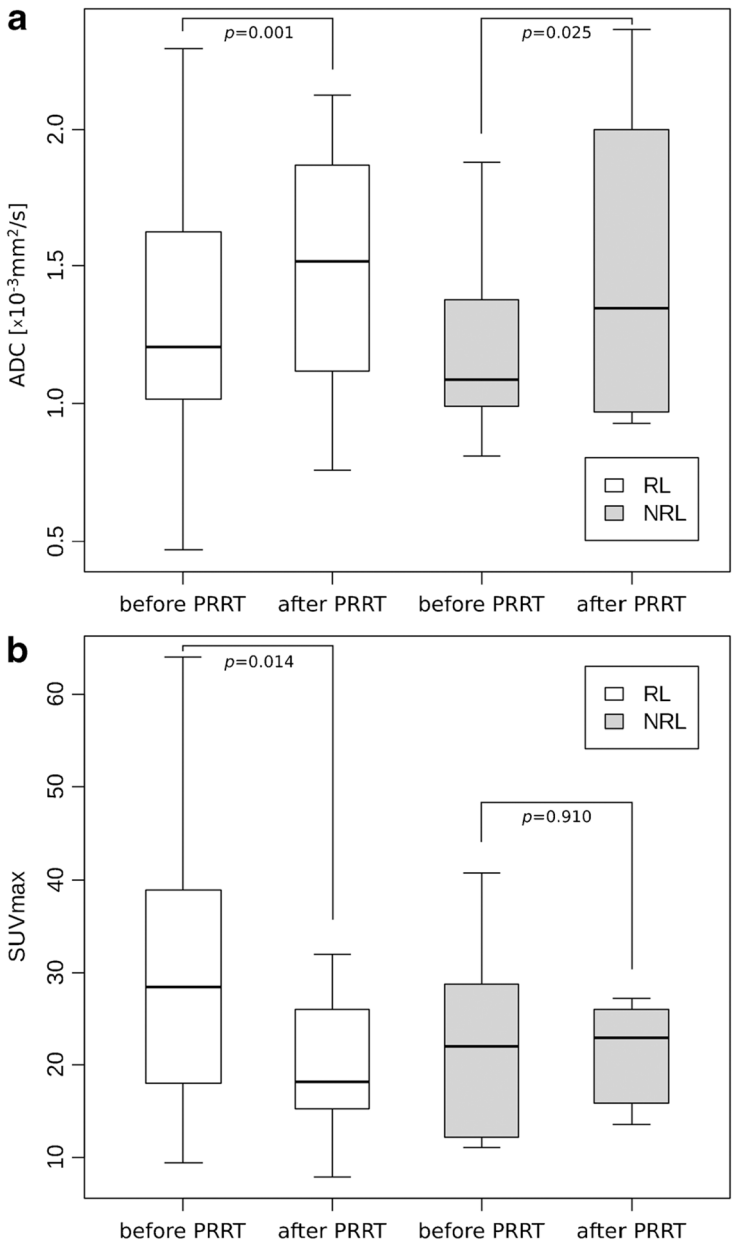

Fig. 1.

a–b *Box-and-whisker plots* (*box* first and third quartile, *whisker* minimum and maximum of all data) showing comparison of ADC_{mean} values before and after PRRT (**a**) and maximal SUVs of ^{68}Ga-DOTATOC before and after PRRT (**b**) in responding and nonresponding hepatic lesions of 14 patients suffering frommetastasized GEP-NET. No significant change of SUV_{max} could be observed in NRL after therapy.

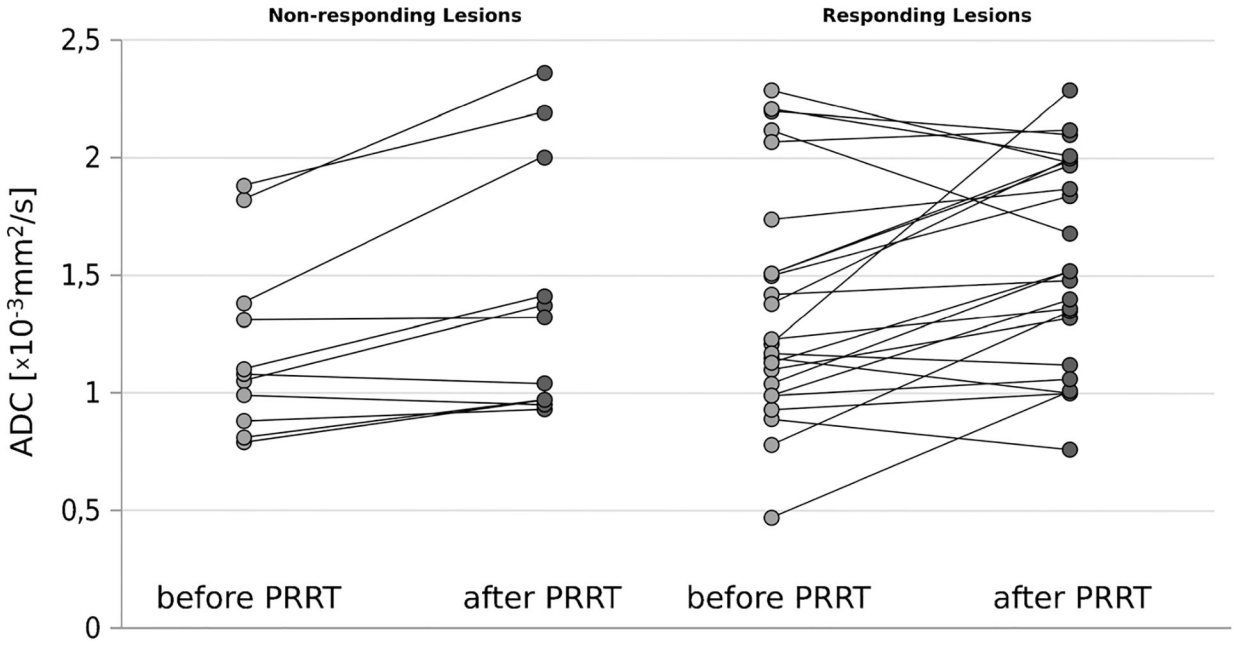

Fig. 2.

ADC_{mean} of nonresponding lesions before and after PRRT (*left*) and responding lesions before and after PRRT (*right*). In both presented subgroups, the median ADC_{mean} value was found to be lower prior to PRRT compared to the ADC_{mean} value after intervention. Seven target lesions in the responding subgroup declined in ADC_{mean} after therapy (mean change, −26.8 %).

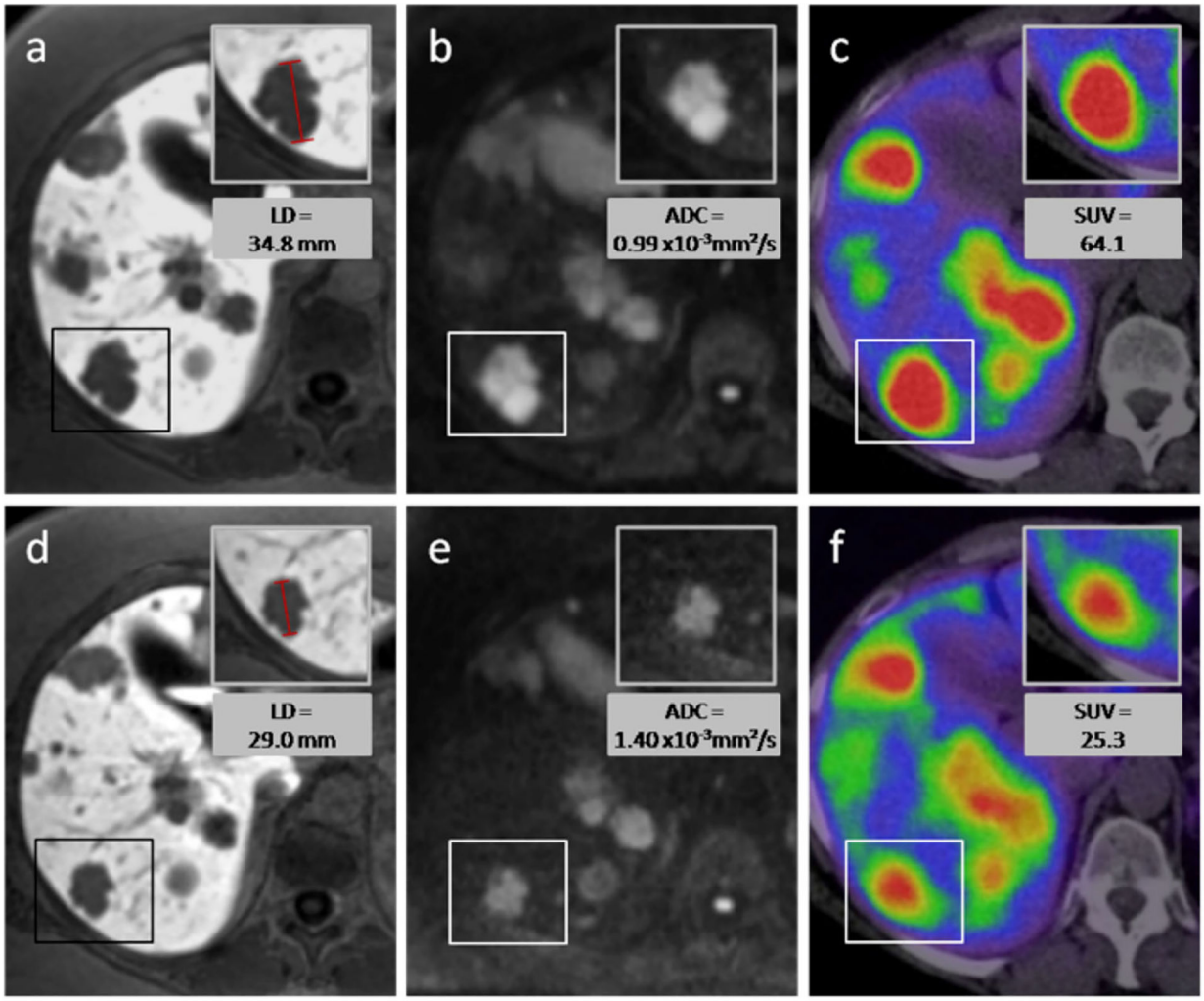

Fig. 3.

Responding lesion—a 54-year-old female with hepatic metastases from a pancreatic NET. After two cycles of intraarterial PRRT with 4 GBq ^{90}Y- and ^{177}Lu-DOTATOC, the longest diameter of the target lesion (*box*) decreased as can be seen on MR images with the hepatocyte-specific contrast agent Gd-EOB-DTPA (**a, d**). The volume of the lesion decreased from 11.0 to 5.0 cm^3. On diffusion-weighted MRI (**b, e**) an increase of ADC_{mean} from 0.99×10 to 1.40×10^{-3} mm^2/s was measured, while the SUV_{max} on ^{68}Ga-DOTATOC-PET/CT decreased from 64.0 to 25.3. *Upper row of figures* images before PRRT, *lower row* images after PRRT.

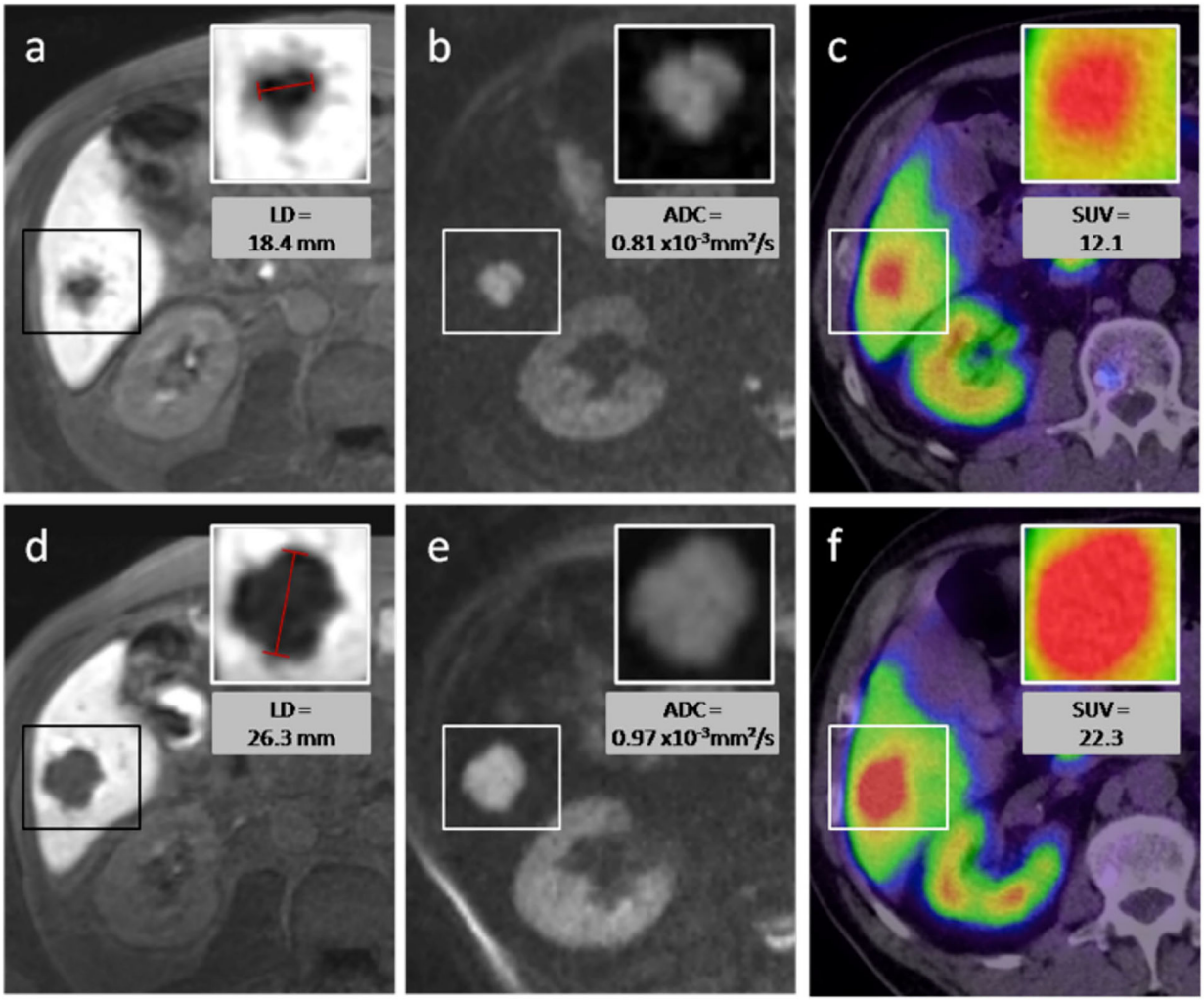

Fig. 4.

Nonresponding lesion—a 65-year-old male patient with caecal NET and hepatic metastasis. After one cycle of intraarterial PRRT with 4 GBq ^{90}Y- and ^{177}Lu-DOTATOC, the longest diameter of the target lesion (*box*) increased as seen on MR images with the hepatocyte-specific contrast agent (**a, d**). The volume of the lesion increased from 2.4 to 8.0 cm^3. On diffusion-weighted MRI (**b, e**), an increase of ADC_{mean} from 0.81×10^{-3} to 0.97×10^{-3} mm^2/s was measured, while the SUV_{max} in ^{68}Ga-DOTATOC-PET/CT increased from 12.1 to 22.3. *Upper row of figures* images before PRRT, *lower row* images after PRRT.

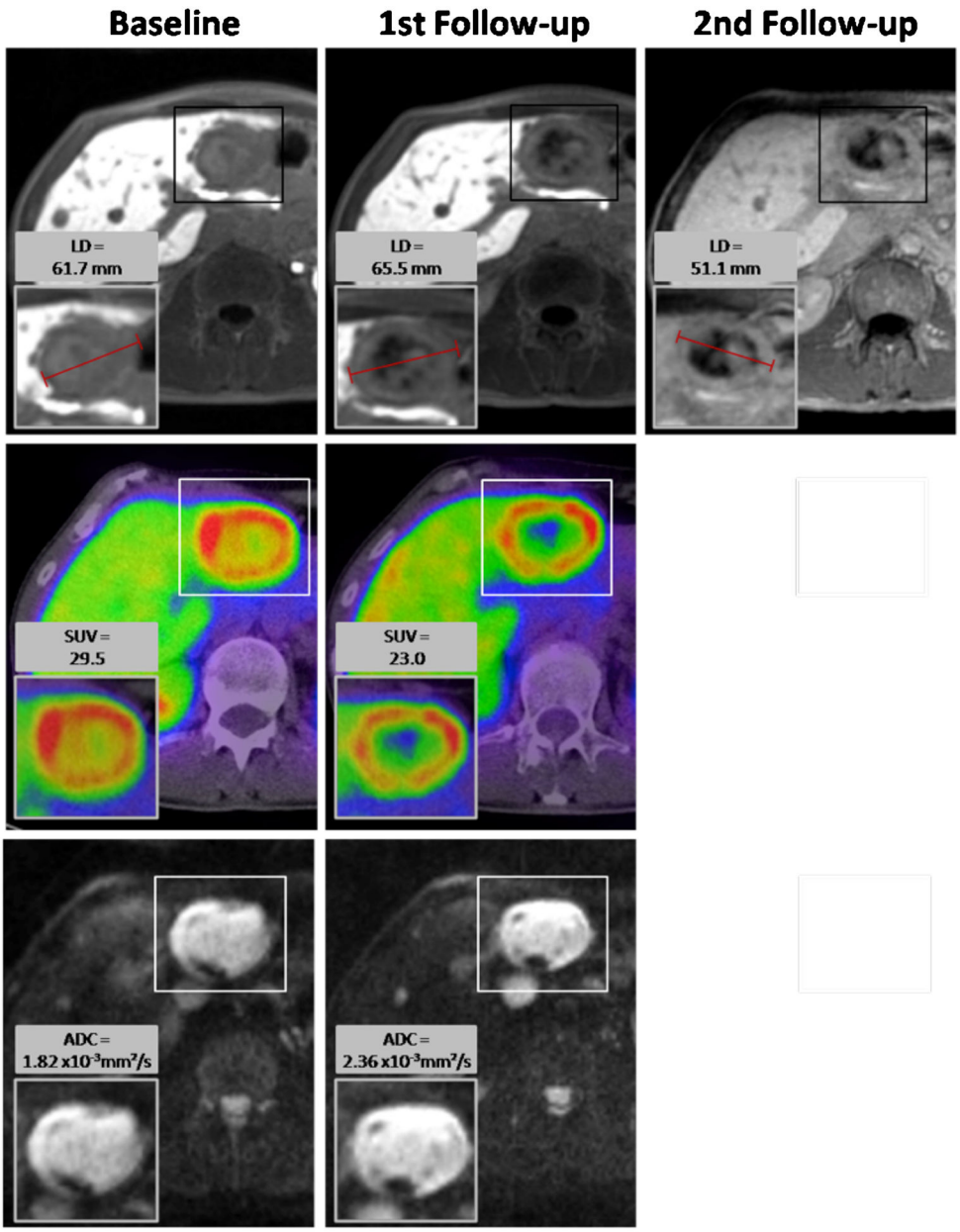

Fig. 5.

Neuroendocrine liver metastasis in a 44-year-old male. After one cycle of PRRT (first follow-up), the LD and the volume of the target lesion increased and it was thus categorized as nonresponding lesion. ADC_{mean} increased from 1.82×10^{-3} to 2.36×10^{-3} mm^2/s. Remarkably, there was a decrease in maximal SUV of ^{68}Ga-DOTATOC in this first follow-up imaging from 29.5 to 23.0. To confirm if this decrease was followed by a later decline in LD and volume of the metastasis after further PRRT, a second follow-up examination was analyzed 11 months after baseline imaging. Here, the size of the target lesion had decreased below its baseline values.

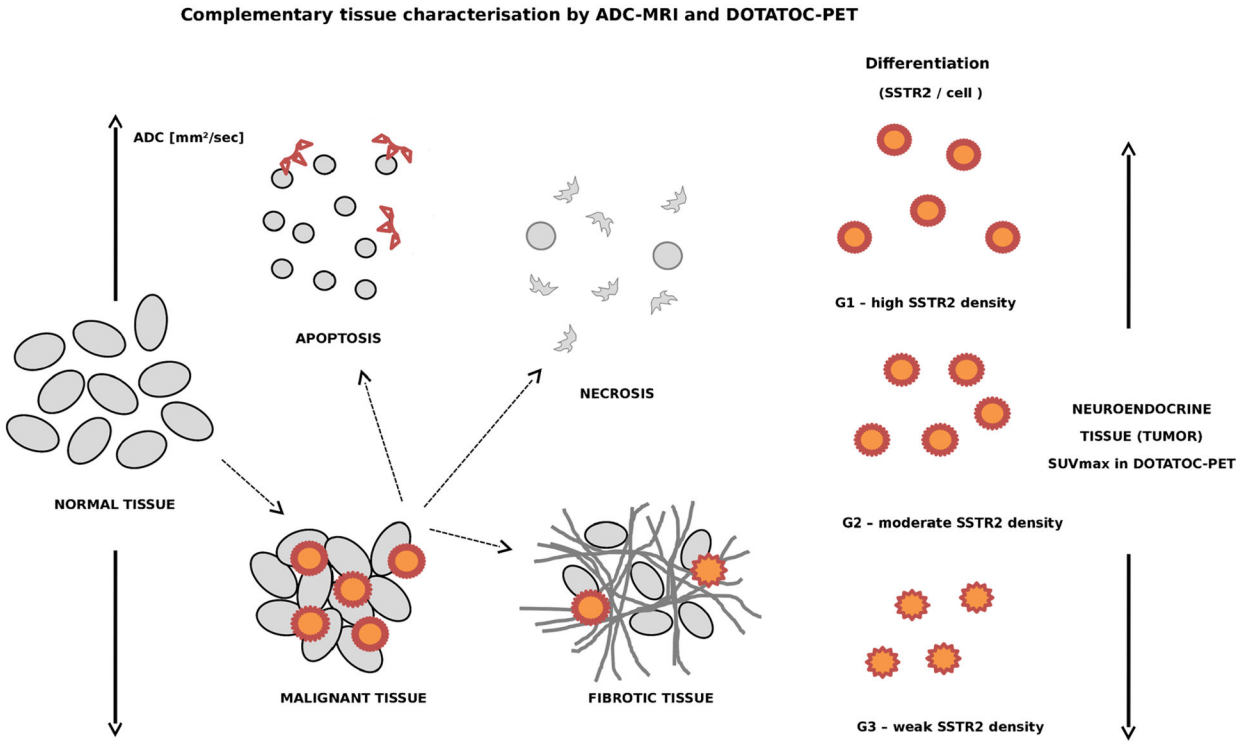

Fig. 6.

Complementary tissue characterisation by DW-MRI and DOTATOC-PET—ADC depends on cell density. Changes with apoptosis or necroses to higher values whereas high density of tumor cells or fibrotic tissue can translate to low ADC values. In contrast, the SUV_{max} in DOTATOC-PET depends on the density of SSTR on cell surface (correlates to grading), the density of tumor cells within a given tumor volume and accessibility of the receptors for the tracer (depends on intratumoral pressure).

Table 1.

Overview over changes in LD, Vol, ADC_{mean}, and SUV_{max} during therapy in RL and NRL

	LD/Vol	ADC_{mean}	SUV_{max}
Responding lesions RL	↓	↑	↓
Nonresponding lesions NRL	↑	↑	

No significant changes in SUV_{max} between baseline and follow-up PET/CT of NRL

Arrows significant changes